arXiv:1405.7128v1 [cond-mat.mes-hall] 28 May 2014

Effects of nitrogen-doping configurations with vacancies on conductivity in graphene

T.M. Radchenko[a,*], V.A. Tatarenko[a], I.Yu. Sagalianov[b], Yu.I. Prylutskyy[b]

[a] *Department of Solid State Theory, G.V. Kurdyumov Institute for Metal Physics of NASU, 36 Acad. Vernadsky Blvd., Kyiv, Ukraine*
[b] *Taras Shevchenko National University of Kyiv, 64 Volodymyrska Str., Kyiv, Ukraine*

Abstract

We investigate electronic transport in the nitrogen-doped graphene containing different configurations of point defects: singly or doubly substituting N atoms and nitrogen–vacancy complexes. The results are numerically obtained using the quantum-mechanical Kubo–Greenwood formalism. Nitrogen substitutions in graphene lattice are modelled by the scattering potential adopted from the independent self-consistent *ab initio* calculations. Variety of quantitative and qualitative changes in the conductivity behaviour are revealed for both graphite- and pyridine-type N defects in graphene. For the most common graphite-like configurations in the N-doped graphene, we also consider cases of correlation and ordering of substitutional N atoms. The conductivity is found to be enhanced up to several times for correlated N dopants and tens times for ordered ones as compared to the cases of their random distributions. The presence of vacancies in the complex defects as well as ordering of N dopants suppresses the electron–hole asymmetry of the conductivity in graphene.

Keywords: graphene, quantum transport, point defects
PACS: 81.05.ue, 72.80.Vp, 72.10.Fk
2014 MSC: 81U35

1. Introduction

Among the currently known and already experimentally implemented or prospective substitutional dopants in graphene films (*e.g.*, B [1, 2, 3, 4, 5, 6, 7], N [5, 6, 7, 8, 9, 10, 11, 12, 13, 14], Al–S [15, 16, 17], Sc–Zn [18, 19, 20, 21], Pt [21, 22], Au [21, 22], Bi [23]), nitrogen (along with boron) is an archetypical natural candidate because its incorporation in graphene lattice requires minor structural perturbations due to its atomic size close to C. The N doping offers an effective way to tailor the properties of graphene and thereby makes

*Corresponding author
Email address: tarad@imp.kiev.ua (T.M. Radchenko)

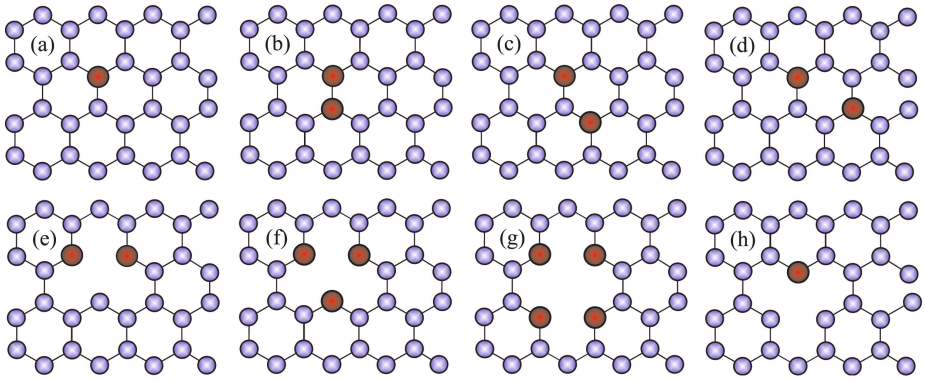

Figure 1: (Colour online) (a)–(d) Graphite- (substitutional) and (e)–(h) pyridine-type defects in graphene lattice. N atoms substitute C ones (a) singly, (b)–(d) doubly or form complex (e) dimerized, (f) trimerized, (g) tetramerized, or (h) monomeric defects with vacancies. Doubly substituting N atoms belong to the same sublattice (c) or different ones (b), (d).

it a promising material for applications in field-effect transistor devices, solar and fuel cells, lithium ion batteries, ultracapacitors, biosensing, field emission, transparent electrodes, or high-performance photocatalysts (see Ref. [24] and references therein).

A series of experiments on structural variety of N-related defects in graphene [6, 7, 8, 9, 10, 11] showed that its rich electronic properties are dependent on how the N-doping configurations are formed: as single (Fig. 1(a)) or double (Figs. 1(b)–1(d)) substitutions or as nitrogen–vacancy complexes comprising monovacancies (Figs. 1(e), 1(f), 1(h)) or divacancies (Fig. 1(g)). Single and double substitutions give rise to the electron-donor-like states and then to n-type doping, while complex defects with vacancies exhibit a hole-acceptor-like character, *i.e.* p-type doping [6, 9, 10]. Both graphite- and pyridine-type defects in Fig. 1 can be observed in graphene films, which are fabricated by chemical vapour deposition growth on different substrates [7, 9, 11]. Formation-energy calculations [12] indicate that graphitic defects in Fig. 1(a) are energetically favoured (stable) among the possible N-doping configurations in Fig. 1. Pyridine-like configurations in Figs. 1(e)–1(h) have higher formation energy, but are stable in the presence of both doping N atoms and vacancies attracting each other and increasing probability of their mutual generation [13]. The first numerical study of charge transport in N-doped graphene [25] deals with the most simple case of random distribution of singly substituting N atoms (Fig. 1(a)). However, in order to regulate the transport properties of graphene by chemical N-doping, it is important to consider all configurations of the N-related defects currently revealed in experiments.

In a given paper, we report on how such diverse N-doping configurations affect the conductivity in single-layer graphene sheet, using an exact numerical technique based on the Kubo–Greenwood formalism appropriate for realistic samples with millions of atoms (the size of our computational domain is 1700000

sites that corresponds to 210×210 nm^2). We also focus on random, correlated, and ordered distributions of N dopants in one of the most common doping configurations, which is found [10] to be singly substituting N atom in Fig. 1(a).

2. Tight-binding model along with Kubo–Greenwood formalism

To investigate charge transport in the N-doped graphene, a real-space numerical implementation within the Kubo–Greenwood formalism [26, 27], which captures all (ballistic, diffusive, and localization) transport regimes, is employed. Within this approach, the energy (E) and time (t) dependent transport coefficient, $D(E,t)$ [30], is governed by the wave-packet propagation [26, 27]: $D(E,t) = \left\langle \Delta \hat{X}^2(E,t) \right\rangle / t$, where the mean quadratic spreading of the wave packet along the direction x reads as [26, 27]

$$\left\langle \Delta \hat{X}^2(E,t) \right\rangle = \frac{\mathrm{Tr}[(\hat{X}(t) - \hat{X}(0))^2 \delta(E - \hat{H})]}{\mathrm{Tr}[\delta(E - \hat{H})]} \tag{1}$$

with $\hat{X}(t) = \hat{U}^\dagger(t)\hat{X}\hat{U}(t)$—the position operator in the Heisenberg representation, $\hat{U}(t) = e^{-i\hat{H}t/\hbar}$—the time-evolution operator, and a standard p-orbital nearest-neighbour tight-binding Hamiltonian $\hat{H}$ is [28, 29]

$$\hat{H} = -u \sum\nolimits_{i,i'} c_i^\dagger c_{i'} + \sum\nolimits_i V_i c_i^\dagger c_i, \tag{2}$$

where $c_i^\dagger$ (c_i) is a standard creation (annihilation) operator acting on a quasiparticle at the site i. The summation over i runs the entire honeycomb lattice, while i' is restricted to the sites next to i; $u = 2.7$ eV is the hopping integral for the neighbouring C atoms occupying i and i' sites at a distance $a = 0.142$ nm between them; and V_i is the on-site potential describing scattering by the N dopants.

The impurity scattering potential in the Hamiltonian matrix is introduced as on-site energies V_i varying with distance r to the impurity N atom at the site i according to the potential profile $V = V(r) < 0$ in Fig. 2 adopted from the self-consistent *ab initio* calculations [31]. As fitting shows, this potential is far from the Coulomb- or Gaussian-like shapes commonly used in the literature for charged impurities in graphene, while two-exponential fitting exactly reproduces the potential. Such a scattering potential presents both short-range and some long-range features [25]. A vacancy can be regarded as a site with hopping parameters to other sites being zero (note that another way to model vacancy at the site i is $V_i \to \infty$) [32]. In our numerical simulations, we implement a vacancy removing the atom at the vacancy site.

The dc conductivity σ can be extracted from the diffusivity $D(E,t)$, when it saturates reaching the maximum value, $\lim_{t\to\infty} D(E,t) = D_{\max}(E)$, and the diffusive transport regime occurs. Then the semiclassical conductivity at a zero temperature is defined as [26, 27]

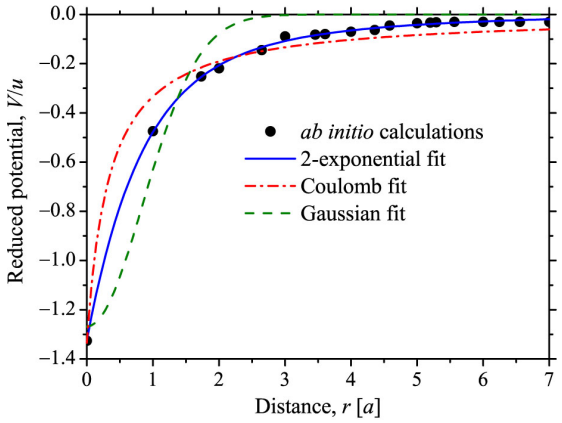

Figure 2: (Colour online) Scattering potential (•) adopted from Ref. [31] and fitted by different functions: Gaussian-like ($V = Ue^{-r^2/2\xi^2}$ with fitting parameters $U = -1.27u$ and $\xi = 0.85a$ standing here as a maximal potential height and an effective potential radius, respectively), Coulomb-like ($V = U/(\xi + r)$ with $U = -0.44ua$ and $\xi = 0.33a$), and two-exponential ($V = U_1 e^{-r/\xi_1} + U_2 e^{-r/\xi_2}$ with $U_1 = -1.07u$, $\xi_1 = 0.79a$, $U_2 = -0.25u$, $\xi_2 = 2.72a$).

$$\sigma = e^2 \tilde{\rho}(E) D_{\max}(E), \tag{3}$$

where $-e < 0$ denotes the electron charge and $\tilde{\rho}(E) = \rho/\Omega = \mathrm{Tr}[\delta(E - \hat{H})]/\Omega$ is the density of sates (DOS) per unit area Ω (and per spin). The DOS is also used to calculate the electron density as $n_e(E) = \int_{-\infty}^{E} \tilde{\rho}(E)dE - n_{\mathrm{ions}}$, where $n_{\mathrm{ions}} = 3.9 \cdot 10^{15}$ cm^{-2} is the density of the positive ions in the graphene lattice compensating the negative charge of the p-electrons (at the neutrality (Dirac) point of pristine graphene, $n_e(E) = 0$). Combining the calculated $n_e(E)$ with $\sigma(E)$, we compute the density dependence of the conductivity $\sigma = \sigma(n_e)$.

Note that we do not go into details of numerical calculations of DOS, $D(E, t)$, and σ since details of the computational method we utilize here (Chebyshev method for solution of the time-dependent Schrödinger equation, calculation of the first diagonal element of the Green's function using continued fraction technique and tridiagnalization procedure of the Hamiltonian matrix, averaging over the N and vacancy realizations, sizes of initial wave packet and computational domain, boundary conditions, etc.) are given in Ref. [27].

3. Results and discussion

Figure 3 demonstrates the electron-density dependent conductivity for defect configurations depicted in Fig. 1. To compare conductivity curves, we chose two representative concentrations of the point nitrogen-related defects: $n_d = n_{\mathrm{N}} + n_v = 1\%$ and $n_d = 3\%$, where n_{N} and n_v are nitrogen and vacancy relative concentrations, respectively. In case of the graphitic defects, concentration of

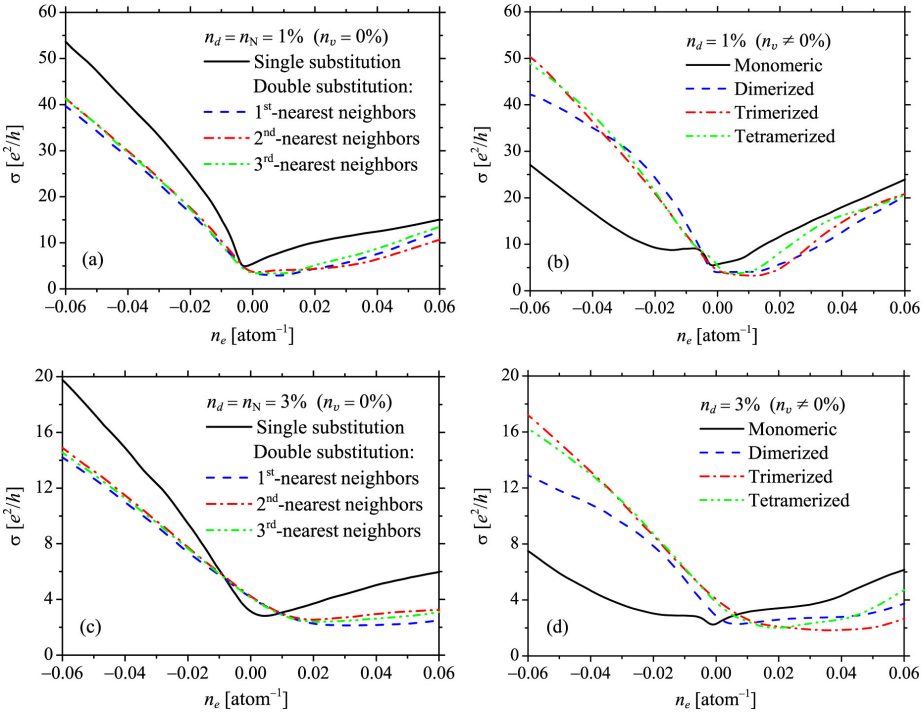

Figure 3: (Colour online) Conductivity vs. the electron density for 1% (a), (b) and 3% (c), (d) of point N-related defects with graphite- (a), (c) and pyridine-like (b), (d) arrangements represented in Fig. 1.

point defects n_d equals with concentration of substituting N atoms n_N ($n_d = n_N$), since $n_v = 0$. For the pyridinic defects, the vacancy concentration $n_v \neq 0$ that leads to $n_N = n_v = n_d/2$ for monomeric defects; $n_N = 2n_d/3$ and $n_v = n_d/3$ for dimerized as well as tetramerized defects; $n_N = 3n_d/4$ and $n_v = n/4$ for trimerized defects.

It is evidently from Fig. 3 that different configurations of N-related defects in graphene affect its conductivity both quantitatively and qualitatively. Specifically, comparing conductivity for single and double N substitutions in Figs. 3(a) and 3(c) the following is noteworthy. For double substitutions, the Fermi level is more strongly shifted away from the Dirac point to the side of positive energies E corresponding to the n-type charge carriers. The dependence $\sigma = \sigma(n_e)$ being sublinear for singly substituting N dopants transforms into linear one for double substitutions. Double substitutions result to the degradation of conductivity: particularly, σ is decreased by up to $\cong 50\%$ for electron densities n_e away from the Dirac point (Fig. 3(b)). However, conductivity is not practically dependent on how pairs of N atoms are positioned: as first-, second-, or third-nearest neighbours. (Note that abundant amount of double substitutions of the second-nearest neighbouring N atoms within the same sublattice have been confirmed

experimentally and theoretically in Ref. [11].)

Behaviours of conductivity in graphene with nitrogen–vacancy complexes (Figs. 3(b) and 3(d)) are more complicated as compared with those seen in Figs. 3(a) and 3(c) for graphitic defects, since the $\sigma = \sigma(n_e)$ curves are dependent not only on the type of defects, their density, and configuration, but on the type (p or n) of charge carriers. For electron densities n_e, all dependencies $\sigma = \sigma(n_e)$ in Figs. 3(b) and 3(d) are almost sublinear or superlinear for smaller (1%) and larger (3%) defect concentrations, respectively; while for hole densities $-n_e > 0$, $\sigma = \sigma(n_e)$ is linear, sublinear, or superlinear, depending on the type of pyridine-like configurations. Such a behaviour is caused by the more complex defect configurations due to the presence of simple vacancies or divacancies. One can see from Fig. 3(d) that for hole densities ($-n_e > 0$), which contribute to the dominant p-type conductivity for pyridinic defects, the larger relative content of vacancies (n_v), the degraded the conductivity for the same total concentration of point defects (n_d). The same effect is seen in Fig. 3(b) at least for large hole densities. These results agree with formation-energy (stability) calculations [12] reported that graphite-like configuration is the most stable; trimerized and tetramerized defects are less stable and have small formation-energy difference; dimerized defects are much less stable; at last, monomeric defects have the lowest stability energy among the all N-doped defects in graphene.

The observed asymmetry of the conductivity curves with respect to the neutrality point (Fig. 3) follows from the nature of the scattering potential, which impacts differently electrons and holes due to its asymmetric property: $V < 0$. The presence of vacancies suppresses the electron–hole asymmetry in the conductivity. This effect manifests itself for monomeric cases in Figs. 3(b) and 3(d), where the relative vacancy concentration with respect to the nitrogen one is the largest among the variety of complex defects in Figs. 1(e)–1(h).

Among the represented configurations of N-related defects in Fig. 1, substitutional (graphite-like) ones are found to be the most common ($\cong$ 75–80% dominance among all defects identified) [10, 11]. Further, we deal with a case of singly substituting N atoms for their random (Fig. 4(a)), correlated (Fig. 4(b)), and ordered (Fig. 4(c)) distributions over the honeycomb-lattice sites.

In case of correlation (Fig. 4(b)), N impurity atoms are no longer considered to be randomly located. To describe their spatial correlation, we adopt a model [33] using the pair distribution function $p(\mathbf{R}_i - \mathbf{R}_j) \equiv p(r)$:

$$p(r) = \begin{cases} 0, & r < r_0 \\ 1, & r \geq r_0 \end{cases} \tag{4}$$

where $r = |\mathbf{R}_i - \mathbf{R}_j|$ is a distance between the two N atoms, and the correlation length r_0 defines minimal distance that can separate any two of them. Note, that for the randomly distributed impurities, $r_0 = 0$. The largest distance $r_{0_{\max}}$ depends on the relative nitrogen concentration n_{N}; in our calculations for $n_{\mathrm{N}} = 3.125\%$, we chose $r_0 = r_{0_{\max}} = 5a$.

In case of ordering (Fig. 4(c)), we consider structure in Fig. 4(d), where the relative content of ordered N atoms is $n_{\mathrm{N}} = 1/32 = 3.125\%$. This struc-

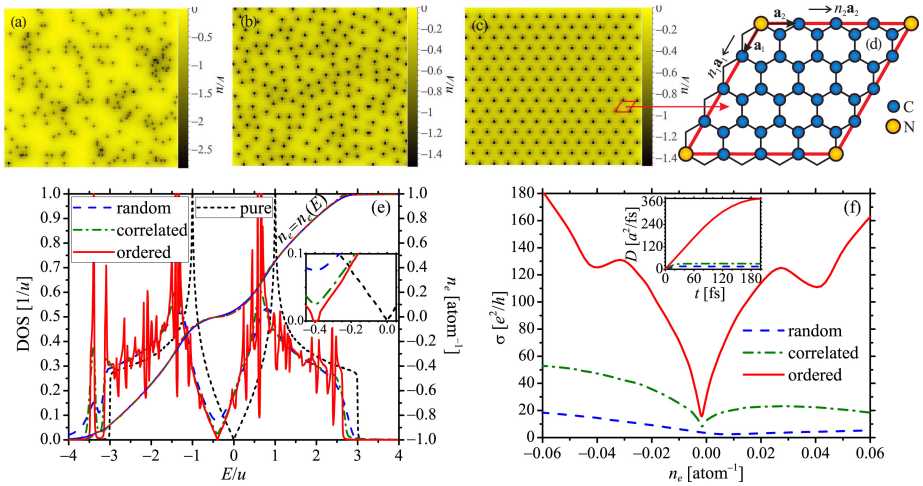

Figure 4: (Colour online) (a)–(c) Scattering potential distributions, (e) density of states (DOS), and (f) electron-density dependent conductivity for $n_{\rm N} = 3.125\%$ of (a) random, (b) correlated, and (c)–(d) ordered nitrogen substitutions in graphene lattice. Ordered N atoms (c) form superstructure with one N atom within the primitive unit cell (d). Inset in (e): zoom of DOS in the band gap and zero energy regions. Inset in (f): diffusivity vs. the time at the energy $E = 0.2u$ for random, correlated, and ordered N atoms.

ture forms a $C_{31}N$-type superstructure, where distribution of N atoms over the honeycomb-lattice sites can be described by the single-site occupation-probability function derived by the static concentration wave method [34, 35]. In the computer implementation, $n_{\rm N} = 3.125\%$ of N atoms occupy sites within the same sublattice and can be described via a single-site function:

$$P(\mathbf{R}) = \begin{cases} 1, & n_1 + n_2 = 4\mathbb{Z} \\ 0, & \text{otherwise} \end{cases} \tag{5}$$

where n_1, n_2, and $\mathbb{Z}$ belong to the set of integers, and n_1 and n_2 denote coordinates of sites in an oblique coordinate system formed by the basis translation vectors $\mathbf{a}_1$ and $\mathbf{a}_2$ shown in Fig. 4(d).

Figure 4(e) shows the DOS and the electron density $n_e = n_e(E)$ in graphene with $n_{\rm N} = 3.125\%$ of random, correlated, and ordered distributions of N impurity atoms. The Fermi level is shifted with respect to $E = 0$, which is related to negativity of the scattering potential. The calculated DOS-curves for random, correlated, and ordered N atoms are similar with different that peaks appearing at $-4 \lesssim E/u \lesssim -3$ for correlation and manifesting themselves in whole energy interval for ordering. Such peaks in DOS are due to the periodicity of scattering-potential distribution, which describes ordered positions of N atoms in graphene-based superstructure in Fig. 4(d). (Additional calculations [36] showed that the peaks become stronger and even transform into discrete energy levels with broadening as impurity concentration and/or periodic potential increase.) Small band gap for ordered N configurations (see inset in Fig. 4(e)) is

caused by periodic potential (Fig. 4(c)) resulting to ordered distribution of N atoms over the sites of the same sublattice (Fig. 4(d)), *i.e.* to breaking of symmetry of two graphene sublattices. Such a band gap opening due to superlattice of dopants has already been discussed, *e.g.*, in Refs. [37, 38, 39]. Belonging of ordered N dopants to one sublattice also leads to the band gap appearance in graphene electronic spectrum even for a random distribution of the N dopants [40].

In contrast to the cases of random and correlated N atoms, when steady diffusive regime is reached, for the case of ordering a quasi-ballistic regime is observed for a long time as it is shown in the inset of Fig. 4(f). This (quasi-balistic) behaviour of $D(t)$ indicates a very low scattered electronic transport, since electrons live mainly in the sublattice that does not contain the ordered N atoms [40]. If the diffusive regime is not completely reached, the semiclassical conductivity cannot be in principle defined. However we extracted σ for the case of ordered N atoms using the highest $D(t)$ when quasi-ballistic behaviour turns to a quasi-diffusive regime with an almost saturated diffusivity coefficient.

One can see from Fig. 4(f) that correlation and ordering of N dopants rise the conductivity up to several ($\cong$ 3–6) and tens ($\cong$ 20–30) times, respectively, as compared with their random distribution. We predict that such increasing of the conductivity due to the spatial correlation of impurities should manifest in a varying degree for any asymmetric ($V > 0$ or $V < 0$) scattering potential modelling charged impurities or neutral adatoms. However, for symmetric potential ($V \gtrless 0$), correlation does not affect the conductivity in graphene sheets [27]. Note that correlation effect (for potassium impurity atoms in graphene) have been already observed in experiment [41] and sustained in theoretical predictions based on the standard semiclassical Boltzmann approach within the Born approximation [42]. Figure 4(f) demonstrates that ordering of N impurity atoms also suppresses the electron–hole asymmetry of the conductivity, at least, for small charge-carrier densities.

4. Conclusions

The variety of different experimentally-revealed configurations of nitrogen impurity atoms in both graphite- and pyridine-type defects in graphene affects its conductivity quantitatively and qualitatively that we numerically demonstrated using the quantum-mechanical Kubo–Greenwood approach. Charge-carrier-density dependence of the conductivity, $\sigma = \sigma(n)$, can be linear, sublinear, or superlinear depending on relative concentrations of N dopants and vacancies, their configurations over the graphene-lattice sites, and type of carriers—electrons or holes. For the most common graphitic defects, N atoms doubly substituting C ones in graphene degrade its conductivity as compared with their single substitutions. The presence of vacancies in the complex defects as well as ordering of substitutional N atoms suppresses the electron–hole asymmetry of the conductivity. Correlated and ordered N scatterers in graphene modelled by the negative scattering potential enhance the conductivity up to the several and

tens times, respectively, as compared with their random distribution. Demonstrated influences of the various N-doping configurations, especially ordering effect and herewith band gap opening, in the N-doped graphene suggest the possibility of tailoring graphene transport properties via the positioning neutral adatoms or charged impurities on the substrate.

Acknowledgements

T.M.R. benefited immensely from collaboration with Igor Zozoulenko and Artsem Shylau, and thank Sergei Sharapov, Valery Gusynin, Vadim Loktev, and Maksym Strikha for discussions. Yu.I.P. is grateful to DAAD for support.

References

[1] Z.-H. Sheng, H.-L. Gao, W.-J. Bao, F.-B. Wang, X.-H. Xia, J. Mater. Chem. 22 (2012) 390.

[2] W. Norimatsu, K. Hirata, Y. Yamamoto, S. Arai, M. Kusunoki, J. Phys.: Condens. Matter. 24 (2012) 314207.

[3] H. Wang, Y. Zhou, D. Wu, L. Liao, S. Zhao, H. Peng, Z. Liu, Small 9 (2013) 1316.

[4] J. Gebhardt, R.J. Koch, W. Zhao, O. Hofert, K. Gotterbarm, S. Mammadov, C. Papp, A. Gorling, H.-P. Steinruck, Th. Seyller, Phys. Rev. B 87 (2013) 155437.

[5] L.S. Panchakarla, K.S. Subrahmanyam, S.K. Saha, A. Govindaraj, H.R. Krishnamurthy, U.V. Waghmare, C.N.R. Rao, Adv. Mater. 21 (2009) 4726.

[6] B. Zheng, P. Hermet, L. Henrard, ACS Nano7 (2010) 4165.

[7] L. Zhao, M. Levendorf, S. Goncher, T. Schiros, L. Pálová, A. Zabet-Khosousi, K.T. Rim, Ch. Gutiérrez, D. Nordlund, C. Jaye, M. Hybertsen, D. Reichman, G.W. Flynn, J. Park, A.N. Pasupathy, Nano Lett. 13 (2013) 4659.

[8] B. Guo, Q. Liu, E. Chen, H. Zhu, L. Fang, J.R. Gong, Nano Lett. 10 (2010) 4975.

[9] D. Wei, Y. Liu, Y. Wang, H. Zhang, L. Huang, G. Yu, Nano Lett. 9 (2009) 1752.

[10] F. Joucken, Y. Tison, J. Lagoute, J. Dumont, D. Cabosart, B. Zheng, V. Repain, C. Chacon, Y. Girard, A.R. Botello-Mendez, S. Rousset, R. Sporken, J.-Ch. Charlier, L. Henrard, Phys. Rev. B 85 (2012) 161408(R).

[11] R. Lv, Q. Li, A.R. Botello-Méndez, T. Hayashi, B. Wang, A. Berkdemir, Q. Hao, A. L. Elías, R. Cruz-Silva, H. R. Gutiérrez, Y.A. Kim, H. Muramatsu, J. Zhu, M. Endo, H. Terrones, J.-Ch. Charlier, M. Pan, M. Terrones, Sci. Rep. 2 (2012) 586.

[12] Y. Fujimoto, S. Saito, Phys. Rev. B 84 (2011) 245446.

[13] Z. Hou, X. Wang, T. Ikeda, K. Terakura, M. Oshima, M.A. Kakimoto, S. Miyata, Phys. Rev. B 85 (2012) 165439.

[14] L. Zhao, R. He, K.T. Rim, T. Schiros, K.S. Kim, H. Zhou, Ch. Gutiérrez, S.P. Chockalingam, C.J. Arguello, L. Pálová, D. Nordlund, M.S. Hybertsen, D.R. Reichman, T.F. Heinz, Ph. Kim, A. Pinczuk, G.W. Flynn, A.N. Pasupathy, Science 333 (2011) 999.

[15] J. Dai, J. Yuan, and P. Giannozzi, Appl. Phys. Lett. 95 (2009) 232105.

[16] J. Dai, J. Yuan, Phys. Rev. B 81 (2010) 165414.

[17] Y.-H. Zhang, Y.-B. Chen, K.-G. Zhou, C.-H. Liu, J. Zeng, H.-L. Zhang, Y. Peng, Nanotechnology 20 (2009) 185504.

[18] E.J.G. Santos, A. Ayuela, D. Sánchez-Portal, New J. Phys. 12 (2010) 053012.

[19] E.J.G. Santos, D. Sanchez-Portal, A. Ayuela, Phys. Rev. B 81 (2010) 125433.

[20] E.J.G. Santos, A. Ayuela, S.B. Fagan, J. Mendes Filho, D.L. Azevedo, A.G. Souza Filho, D. Sanchez-Portal, Phys. Rev. B 78 (2008) 195420.

[21] A.V. Krasheninnikov, P.O. Lehtinen, A.S. Foster, P. Pyykko, R.M. Nieminen, Phys. Rev. Lett. 102 (2009) 126807.

[22] Y. Gan, L. Sun, F. Banhart, Small 4 (2008) 587.

[23] O.Ü. Aktürk, M. Tomak, Appl. Phys. Lett. 96 (2010) 081914.

[24] H. Wang, T. Maiyalagan, X. Wang, ACS Catal. 2 (2012) 781.

[25] A. Lherbier, X. Blase, Y.-M. Niquet, F. Triozon, S. Roche, Phys. Rev. Lett. 101 (2008) 036808.

[26] S. Roche, N. Leconte, F. Ortmann, A. Lherbier, D. Soriano, J.-Ch. Charlier, Solid State Comm. 153 (2012) 1404.

[27] T.M. Radchenko, A.A. Shylau, I.V. Zozoulenko, Phys. Rev. B 86 (2012) 035418.

[28] N.M.R. Peres, Rev. Mod. Phys. 82 (2010) 2673.

[29] S. Das Sarma, S. Adam, E. H. Hwang, E. Rossi, Rev. Mod. Phys. 83 (2011) 407.

[30] $D(E,t)$ has a dimension of diffusivity, nevertheless, it is not a diffusion coefficient in a nondiffusive ballistic regime, when there are no any scatterings.

[31] Ch. Adessi, S. Roche, X. Blase, Phys. Rev. B 73 (2006) 125414.

[32] S. Yuan, H. De Raedt, M.I. Katsnelson, Phys. Rev. B 82 (2010) 115448.

[33] Qiuzi Li, E.H. Hwang, E. Rossi, S. Das Sarma, Phys. Rev. Lett. 107 (2011) 156601.

[34] T.M. Radchenko, V.A. Tatarenko, Physica E 42 (2010) 2047.

[35] A.G. Khachaturyan, Theory of Structural Transformations in Solids, Dover Publications, Minola, NY, 2008.

[36] T. M. Radchenko, V. A. Tatarenko, I. Yu. Sagalianov, Yu. I. Prylutskyy, in Graphene: Mechanical Properties, Potential Applications and Electrochemical Performance, edited by B. T. Edwards, Nova Science Publishers, New York, 2014, p. 219.

[37] C.-H. Park, Li Yang, Y.-W. Son, M. L. Cohen, S.G. Louie, Nature Phys. 4 (2008) 213.

[38] R. Martinazzo, S. Casolo, G.F. Tantardini, Phys. Rev. B 81 (2010) 245420.

[39] S. Casolo, R. Martinazzo, G.F. Tantardini, J. Phys. Chem. C 115 (2011) 3250.

[40] A. Lherbier, A.R. Botello-Mendez, J.C. Charlier, Nano Lett. 13 (2013) 1446.

[41] Jun Yan, M.S. Fuhrer, Phys. Rev. Lett. 107 (2011) 206601.

[42] Qiuzi Li, E.H. Hwang, E. Rossi, S. Das Sarma, Phys. Rev. Lett. 107 (2011) 156601.